Photon migration in turbid media using a cumulant approximation to radiative transfer

M. Xu,* W. Cai, M. Lax, and R. R. Alfano
Institute for Ultrafast Spectroscopy and Lasers, New York State Center of Advanced Technology for Ultrafast Photonics and Department of Physics, The City College and Graduate Center of City University of New York, New York, New York 10031
(Received 1 August 2001; published 18 June 2002)

A photon transport model for light migration in turbid media based on a cumulant approximation to radiative transfer is presented for image reconstruction inside an infinite medium or a bounded medium with a planar geometry. This model treats weak inhomogeneities through a Born approximation of the Boltzmann radiative transfer equation and uses the second-order cumulant solution of photon density to the Boltzmann equation as the Green's function for the uniform background. It provides the correct behavior of photon migration at early times and reduces at long times to the center-moved diffusion approximation. At early times, it agrees much better with the result from the Monte Carlo simulation than the diffusion approximation. Both approximations agree well with the Monte Carlo simulation at later times. The weight function for image reconstruction under this proposed model is shown to have a strong dependence at both early and later times on absorption and/or scattering inhomogeneities located in the propagation direction of and close to the source, or in the field of view of and close to the detector. This effect originates from the initial ballistic motion of incident photons, which is substantially underestimated by the diffusion approximation.

DOI: 10.1103/PhysRevE.65.066609 PACS number(s): 42.25.Dd, 05.60.Cd, 42.30.Wb, 02.70.Uu

I. INTRODUCTION

Photon migration in turbid media is a random walk in which rays or photons traverse a medium of scatterers and absorbers, and undergo multiple scattering and absorption events before escaping. A natural framework to deal with this type of problem is provided by the theory of radiative transfer in Chandrasekhar's classic text [1]. The linear Boltzmann equation governs the radiation field in a medium that absorbs, emits, and scatters radiation [2]. Because the Boltzmann equation is a nonseparable, integro-differential equation of first order for which an exact closed-form solution is not known except for a few special cases, various approximations have been devised [1,3,4]. The most common approximation is the diffusion approximation, which corresponds to the lowest-order truncation in the spherical harmonic expansion of the photon distribution function. It follows from the Boltzmann equation under the assumption that the photon distribution is almost isotropic after a sufficient large number of scattering events, and thus provides an asymptotic approximation applicable to later times [5]. The diffusion approximation is invalid when the incident photon still retains its directionality preference. Moreover, approximations using higher-order truncation in the spherical harmonic expansion of the photon distribution function are still inefficient in describing the ballistic movement of photons at early times [6]. Yoo *et al.* [7] reported that the diffusion approximation fails for small and intermediate scattering ranges. The range of failure is proportional to the transport mean free path $l_t = l_s/(1-g)$ where l_s is the scattering mean free path and g is the scattering anisotropy (the average cosine of the scattering angle). For one important class of applications of photon migration in a turbid medium—the medical applications, the medium has a strongly peaked phase function in the forward direction and a typical transport mean free path $l_t \sim 1$ mm for human breast tissue. The diffusion approximation is thus incorrect for a substantial scattering range. In optical tomography [8–13] where the distribution of inhomogeneities inside a highly scattering medium is reconstructed from measurements of the transmitted light surrounding the medium, the diffusion approximation yields a much underestimated weight function when any separation between the source, the inhomogeneity, and the detector is small. This error may distort the signal from the inhomogeneity inside the medium because the weight function near surface is usually much larger than that inside.

Recently, an analytical solution to the Boltzmann equation was derived by the authors in an infinite uniform medium using a cumulant expansion [14,15]. An exact but formal solution to the Boltzmann equation yields the photon distribution function $I(\mathbf{r},\mathbf{s},t)$ at position $\mathbf{r}$, direction $\mathbf{s}$, and time t,

$$I(\mathbf{r},\mathbf{s},t) = \left\langle \delta\left[\mathbf{r} - c\int_0^t \mathbf{s}(t')dt'\right]\delta(\mathbf{s}(t)-\mathbf{s})\right\rangle, \qquad (1)$$

for a source $\delta(\mathbf{r}-\mathbf{r}_0)\delta(\mathbf{s}-\mathbf{s}_0)\delta(t)$, where $\langle\rangle$ means an ensemble average in photon direction space. Equation (1) is evaluated in Fourier space with the use of the well-known cumulant expansion theorem [16]. An algebraic closed form of expression is obtained for an arbitrary nth order cumulant. This expansion is inherently different from the spherical harmonics expansion of the photon distribution. The first-order cumulant calculation determines the *exact* center position of the photon distribution; the second-order cumulant calculation determines the *exact* half width of the photon distribution in addition; higher-order cumulant calculations provide progressively more details of the shape of the photon distribution but do not modify the cumulants of lower order. This is a major advantage of the cumulant expansion. The photon distribution approaches a Gaussian distribution as the number of scattering events increases according to the central limit theorem [16]. So it is not surprising that the second-order cumulant solution with a correct center position and

*Electronic address: minxu@sci.ccny.cuny.edu

half-width has already provided a clear picture of the time evolution of photon migration from the initial ballistic to the final diffusive regime—that photons migrate with a center that advances in time, and with an ellipsoidal contour that grows and changes shape [14].

The cumulant solution depends explicitly on the phase function of the medium and involves a complicated numerical integration over angular parameters to build a forward model. It is inconvenient for direct use in image reconstruction. An approximate form of the second-order cumulant solution relating the scattered wave field directly to the weak inhomogeneities in an infinite space was later proposed by the authors [17], which retains the main features of photon propagation at both early and later times and reduces to the conventional diffusion approximation at later times.

In this paper, we will first extend the second-order cumulant solution to planar geometries (semi-infinite and slab media) after a brief recount of the main results of the cumulant solution to the Boltzmann equation in an infinite space. The result of Monte Carlo simulations is then presented for both infinite and semi-infinite media to verify the behavior of the second-order cumulant solution at both early and later times. The weight function for image reconstruction of weak inhomogeneities is calculated with use of the simplified cumulant and diffusion approximations for semi-infinite and slab media. The results from the two approximations are compared. The advantage of this model over the diffusion approximation is then discussed.

II. THEORY

The Boltzmann equation for photon distribution function $I(\mathbf{r},\mathbf{s},t)$ at position $\mathbf{r}$, direction $\mathbf{s}$, and time t from a unit source at position $\mathbf{r}_0$ propagating along $\mathbf{s}_0$ at time $t=0$, is given by

$$\frac{\partial}{\partial t}I(\mathbf{r},\mathbf{s},t)+c\mathbf{s}\cdot\nabla_{\mathbf{r}}I(\mathbf{r},\mathbf{s},t)+c[\mu_s(\mathbf{r})+\mu_a(\mathbf{r})]I(\mathbf{r},\mathbf{s},t)$$
$$=c\mu_s(\mathbf{r})\int d\mathbf{s}'P(\mathbf{s},\mathbf{s}')I(\mathbf{r},\mathbf{s}',t)d\mathbf{s}'$$
$$+\delta(\mathbf{r}-\mathbf{r}_0)\delta(\mathbf{s}-\mathbf{s}_0)\delta(t), \quad (2)$$

where c is the speed of light inside the medium, μ_a and μ_s denote the position-dependent absorption and scattering coefficients, and $P(\mathbf{s},\mathbf{s}')$ is the normalized phase function of the light propagation in the medium. The known phase function is assumed to depend only on the scattering angle $\mathbf{s}\cdot\mathbf{s}'$, and is then expandable in Legendre polynomials,

$$P(\mathbf{s},\mathbf{s}')=(4\pi)^{-1}\sum_l a_l P_l(\mathbf{s}\cdot\mathbf{s}'). \quad (3)$$

Equation (2) is nonseparable. However the evolution in direction space, $F(\mathbf{s},t|\mathbf{s}_0)\exp(-\mu_a ct)=\int d^3\mathbf{r}I(\mathbf{r},\mathbf{s},t|\mathbf{r}_0,\mathbf{s}_0)$, obeys a separable equation with the solution [14]

$$F(\mathbf{s},t|\mathbf{s}_0)=(4\pi)^{-1}\sum_l (2l+1)\exp(-g_l t)P_l(\mathbf{s}\cdot\mathbf{s}_0). \quad (4)$$

Here $g_l=c\mu_s[1-a_l/(2l+1)]$, especially $g_0=0$ and $g_1=c\mu_s'$ where μ_s' is the reduced scattering coefficient. The formal solution to the Boltzmann equation, Eq. (1), is then evaluated by (1) expressing its first δ function of position $\mathbf{r}$ as an integral of $\exp[i\mathbf{k}\cdot(\mathbf{r}-c\int_0^t\mathbf{s}(t')dt')]$ over $\mathbf{k}$ in the Fourier space, (2) making a cumulant expansion of the latter, and (3) calculating the cumulants in the direction space with use of the exact Green's function $F(\mathbf{s},t|\mathbf{s}_0)$ [15].

An arbitrary order of cumulant solution can be calculated [15] with higher-order cumulants providing progressively more details about the photon distribution. Because the photon distribution approaches a Gaussian distribution when the number of the scattering events increases regardless of the details of the scattering, a second-order cumulant solution is sufficient at later times. At early times, the photons' spread is narrow compared to the resolution of the detector, hence the detailed shape is less important than the correct position and half-width of the beam. We emphasize the center of the position and half-width obtained from the second-order cumulant solution is *exact* and will not be altered by higher order cumulant solutions.

The second-order cumulant solution of the photon density $N^{(0)}(\mathbf{r},t|\mathbf{r}_0,\mathbf{s}_0)=\int ds I^{(0)}(\mathbf{r},\mathbf{s},t|\mathbf{r}_0,\mathbf{s}_0)$ for an incident source propagating along the positive z axis ($\mathbf{s}_0=\hat{z}$) in a uniform medium, is given by [14]

$$N^{(0)}(\mathbf{r},t|\mathbf{r}_0,\mathbf{s}_0)=\frac{1}{(4\pi D_{zz}ct)^{1/2}}\frac{1}{4\pi D_{xx}ct}$$
$$\times\exp\left\{-\frac{(z-z_0-R_z)^2}{4D_{zz}ct}\right\}$$
$$\times\exp\left\{-\frac{(x-x_0)^2+(y-y_0)^2}{4D_{xx}ct}\right\}$$
$$\times\exp(-\mu_a ct) \quad (5)$$

with a moving center located at

$$R_z=l_t[1-\exp(-ct/l_t)] \quad (6)$$

and the diffusion coefficients

$$D_{xx}=D_{yy}$$
$$=\frac{c}{3t}\left\{\frac{t}{g_1}+\frac{g_2[1-\exp(-g_1t)]}{g_1^2(g_1-g_2)}-\frac{1-\exp(-g_2t)}{g_2(g_1-g_2)}\right\},$$
$$D_{zz}=\frac{c}{3t}\left\{\frac{t}{g_1}-\frac{(3g_1-g_2)[1-\exp(-g_1t)]}{g_1^2(g_1-g_2)}\right.$$
$$\left.+\frac{2[1-\exp(-g_2t)]}{g_2(g_1-g_2)}-\frac{3[1-\exp(-g_1t)]^2}{2g_1^2}\right\}. \quad (7)$$

For simplicity, we use the following approximation to the second-order cumulant solution as the background photon distribution, $I^{(0)}(\mathbf{r},\mathbf{s},t)$, in an infinite uniform medium [17],

$$I^{(0)}(\mathbf{r},\mathbf{s},t|\mathbf{r}_0,\mathbf{s}_0)=N^{(0)}(\mathbf{r},t|\mathbf{r}_0,\mathbf{s}_0)F(\mathbf{s},t|\mathbf{s}_0)$$
$$-\frac{3}{4\pi}D(t)\mathbf{s}\cdot\nabla_{\mathbf{r}}N^{(0)}(\mathbf{r},t|\mathbf{r}_0,\mathbf{s}_0) \quad (8)$$

in building the photon transport model for image reconstruc-

tion where the time-dependent diffusion coefficient $D(t)$ is taken to be an average $D(t)=(D_{xx}+D_{yy}+D_{zz})/3$ of the diffusion coefficient ellipsoid. At early times $t\rightarrow 0$, the first term of Eq. (8) dominates, and $F(\mathbf{s},t|\mathbf{s}_0)\rightarrow\delta(\mathbf{s}-\mathbf{s}_0)$, $D(t)\rightarrow c^2t^2\mu_s'/9\rightarrow 0$, $N^{(0)}(\mathbf{r},t|\mathbf{r}_0,\mathbf{s}_0)\rightarrow\delta(\mathbf{r}-\mathbf{r}_0-c(t-t_0)\mathbf{s}_0)$, thus $I^{(0)}(\mathbf{r},\mathbf{s},t|\mathbf{r}_0,\mathbf{s}_0)$ provides a correct picture of ballistic motion of photons with speed c along the incident direction $\mathbf{s}_0$. At later times, $F(\mathbf{s},t|\mathbf{s}_0)\rightarrow(4\pi)^{-1}$, $D(t)\rightarrow(3\mu_s')^{-1}$, Eq. (8) reduces to the photon distribution of the center-moved diffusion approximation [8].

For weak inhomogeneities, $\delta\mu_a(\mathbf{r})$ and $\delta\mu_s'(\mathbf{r})$, embedded in an otherwise uniform medium, a first-order Born approximation to Eq. (2) yields the change in the photon distribution [17]

$$\delta I(\mathbf{r},\mathbf{s},t|\mathbf{r}_0,\mathbf{s}_0)=-\frac{1}{4\pi}\int dt'\int d\mathbf{r}'c\,\delta\mu_a(\mathbf{r}')N^{(0)}(\mathbf{r}',t-t'|\mathbf{r},-\mathbf{s})N^{(0)}(\mathbf{r}',t'|\mathbf{r}_0,\mathbf{s}_0)+\frac{3c}{4\pi}\int dt'\int d\mathbf{r}'D(t-t')D(t')$$
$$\times[\delta\mu_a(\mathbf{r}')+\delta\mu_s'(\mathbf{r}')]\nabla_{\mathbf{r}'}N^{(0)}(\mathbf{r}',t-t'|\mathbf{r},-\mathbf{s})\cdot\nabla_{\mathbf{r}'}N^{(0)}(\mathbf{r}',t'|\mathbf{r}_0,\mathbf{s}_0)+\frac{3c}{4\pi}\int dt'\int d\mathbf{r}'D(t-t')$$
$$\times[\delta\mu_a(\mathbf{r}')+\delta\mu_s'(\mathbf{r}')]\exp(-c\mu_s't')\{N^{(0)}(\mathbf{r}',t'|\mathbf{r},-\mathbf{s})\mathbf{s}\cdot\nabla_{\mathbf{r}'}N^{(0)}(\mathbf{r}',t-t'|\mathbf{r}_0,\mathbf{s}_0)$$
$$-\mathbf{s}_0\cdot\nabla_{\mathbf{r}'}N^{(0)}(\mathbf{r}',t-t'|\mathbf{r},-\mathbf{s})N^{(0)}(\mathbf{r}',t'|\mathbf{r}_0,\mathbf{s}_0)\} \tag{9}$$

after neglecting fast decaying terms involving $\exp(-2g_lt)$ for $l\geqslant 1$. We should point out that the optical reciprocity relation is satisfied by both the photon density Eq. (5) and the photon distribution Eqs. (8) and (9). At later times, the term in Eq. (9) containing the exponential decay factor $\exp(-c\mu_s't')$ can be neglected, the change in photon density, $4\pi\delta I(\mathbf{r},\mathbf{s},t)$, in the diffusive limit, is reduced to that in the diffusion approximation (Eq. (14) in Ref. [18]).

The restriction of $D(t)$ by taking an average of D_{xx}, D_{yy}, and D_{zz} can be relaxed. The diffusion coefficients $D_{xx}=D_{yy}$ and D_{zz} can be used instead. The only change is to replace all the occurrences of the form of $D(t)\nabla_{\mathbf{r}'}N^{(0)}(\mathbf{r},t|\mathbf{r}_0,\mathbf{s}_0)$ to

$$D_{xx}(t)(\hat{x}\partial/\partial x+\hat{y}\partial/\partial y)N^{(0)}(\mathbf{r},t|\mathbf{r}_0,\mathbf{s}_0)$$
$$+D_{zz}(t)\hat{z}\partial/\partial z'N^{(0)}(\mathbf{r},t|\mathbf{r}_0,\mathbf{s}_0)$$

in both Eqs. (8) and (9).

A. Extension to planar geometries

When the scattering medium is bounded, special conditions are needed to set the photon density at the interfaces. The reflection at the interface reinjects the light into the medium. Using a partial current technique, Zhu *et al.* [19] showed that the boundary condition for a semi-infinite medium can be written as

$$\left[N^{(0)}-z_e\frac{\partial N^{(0)}}{\partial z}\right]_{z=0}=0 \tag{10}$$

at the interface $z=0$ where

$$z_e=\frac{2l_t}{3}\frac{1-R_{\text{eff}}}{1+R_{\text{eff}}}. \tag{11}$$

Here R_{eff} is the effective reflectivity at the interface determined by the Fresnel reflection coefficients. The extrapolation length z_e measures the distance outside the medium where the energy density from the diffusion approximation vanishes linearly. A recent study by Popescu *et al.* [20] has also shown the dependence of the extrapolation length on the scattering anisotropy.

The extrapolated-boundary condition has been successfully employed for planar geometries such as a slab or a semi-infinite medium in diffuse imaging, in which the photon density is set equal to zero at an extrapolated boundary located a distance z_e outside the turbid medium [8,21,22]. The method of images is used to obtain the Green's function in such bounded media. The same technique can be applied here to the Green's function $N^{(0)}(\mathbf{r},t|\mathbf{r}_0,\mathbf{s}_0)$.

Keeping in mind that the source approaches gradually and stops finally at $\mathbf{r}_0+\mathbf{s}_0l_t$ on average with the increase of time, the image of the incident point source at $(x_0,y_0,z_0\geqslant 0)$ propagating along the positive z axis inside a semi-infinite medium with its interface at $z=0$ is a negative one at $(x_0,y_0,-z_0-2z_e-2l_t)$ propagating along the same direction (Fig. 1). At early times, both the source and its image have not arrived at the extrapolated boundary and their contributions at the extrapolated boundary can be neglected. When the time increases, the contributions at the extrapolated boundary from both the source and image tend to cancel each other as both approach their final stops (shadow spots in Fig. 1). The shadow spots just represent the positions of the source and its image in the center-moved diffusion approximation. The Green's function of a semi-infinite medium given by

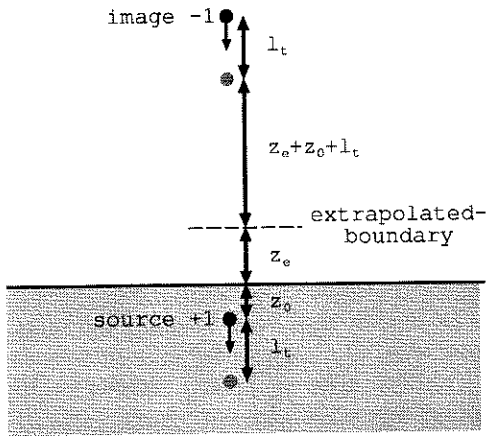

FIG. 1. The incident source at position $(x_0,y_0,z_0\geq 0)$ and its image source at $(x_0,y_0,-z_0-2z_e-2l_t)$ propagating along the positive z axis in a semi-infinite medium $(z\geq 0)$ with its interface at $z=0$. The source and its image move from their original positions (dark spots) to their final stops (shadow spots) at later times.

$$N^{(0)}_{\text{semi}}(\mathbf{r},t|\mathbf{r}_0,\mathbf{s}_0)=N^{(0)}(\mathbf{r},t|x_0,y_0,z_0,\mathbf{s}_0) -N^{(0)}(\mathbf{r},t|x_0,y_0,-z_0-2z_e-2l_t,\mathbf{s}_0) \tag{12}$$

thus approximately satisfies the extrapolated-boundary condition.

The same procedure can be easily applied to a slab with its extrapolated boundaries at $z=0$ and $z=L$. The images of an incident source at (x_0,y_0,z_0) with $0\leq z_0\leq L$ propagating along positive or negative z axis $(s_z=\pm 1)$ are a set of positives images at (x_0,y_0,z_0+2nL) and a set of negative ones at $(x_0,y_0,-z-2nL-2s_zl_t)$, all propagating along the same direction as the source $(-\infty<n<\infty$ is integer).

B. Comparison with the Monte Carlo simulation

We will compare the photon densities computed by the diffusion approximation (DA), the cumulant approximation (CA) Eqs. (5) and (8), and the Monte Carlo method (MC) for an incident collimated pulse first in an infinite space and then in a semi-infinite space. In DA, the incident photons are assumed initially scattered isotropically at a depth of one transport mean free path into the medium as used by Patterson *et al.* [8]. No such adjustments are performed in CA. The Monte Carlo code is adapted from Prahl *et al.* [23] and Wang *et al.* [24]. Photons are launched one by one into the medium. Each photon (regarded as a packet) starts from the origin of the coordinate system and the first scattering event takes place along the positive z axis. The step size (distance between consecutive scattering events) is sampled from an exponential distribution characterized by the total attenuation $\mu_T=\mu_s+\mu_a$, following Beer's law. After each propagation step, the photon packet is split into two parts—a fraction (μ_a/μ_T) is absorbed and the rest scattered. The new propagation direction after scattering (three directional cosines) is sampled by assuming a Henyey-Greenstein phase function [25]. The effect of internal reflection is included in this code. The technique of roulette [26] is used to terminate a photon

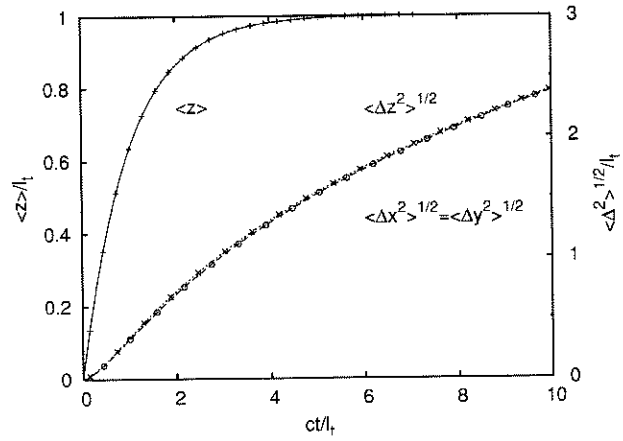

FIG. 2. The center position and the half-width of the photon cloud inside a uniform infinite absorptionless medium with anisotropy equal to 0.9.

packet to improve the efficiency of the calculation without introducing a bias. The results in the following paragraphs have been scaled to use the transport mean free path l_t as the unit of the length and the flight time for one transport mean free path in the medium l_t/c as the unit of the time. The source is incident along the positive z axis at the origin in space and time. 5×10^6 photons are used in one run of the Monte Carlo simulation.

The first- and second-order cumulants (the center position and the half-width of the "photon cloud") of our cumulant solution Eq. (5) is

$$\langle x(t)\rangle=\langle y(t)\rangle=0,\quad \langle z(t)\rangle=l_t[1-\exp(-ct/l_t)],$$
$$\sqrt{\langle\Delta x(t)^2\rangle}=\sqrt{\langle\Delta y(t)^2\rangle}=\sqrt{2D_{xx}(t)ct},$$
$$\sqrt{\langle\Delta z(t)^2\rangle}=\sqrt{2D_{zz}(t)ct}, \tag{13}$$

where $\langle\rangle$ means an ensemble average of photon positions at a specified time. This theoretical prediction can be easily verified by a Monte Carlo simulation. Figure (2) shows the first two cumulants of photons for an incident pulse along the z axis at time zero into an infinite medium with anisotropy 0.9. A perfect agreement on the center position (the first-order cumulant) and the half-width (the second order cumulant) of the photon distribution between our theoretical result and the Monte Carlo simulation is obtained. The half-widths along xyz directions are very close; the value along z direction is a bit larger than that along the xy direction as predicted by Eq. (13).

Figures 3(a)–3(c) shows the photon density at positions $(0,0,3l_t)$, $(0,0,6l_t)$, and $(0,0,10l_t)$ computed by all three different methods for the same infinite medium. At a distance of $3l_t$, the time profile of photon density from the cumulant approximation agrees much better to the Monte Carlo result than DA by providing a correct peak position of photon density. Some amount of photons arriving faster than the speed of light still exist in this second-order cumulant calculation. However, this is already a big improvement compared to DA. The result from CA can be further improved when higher-order cumulants are used. At a larger distance, all the

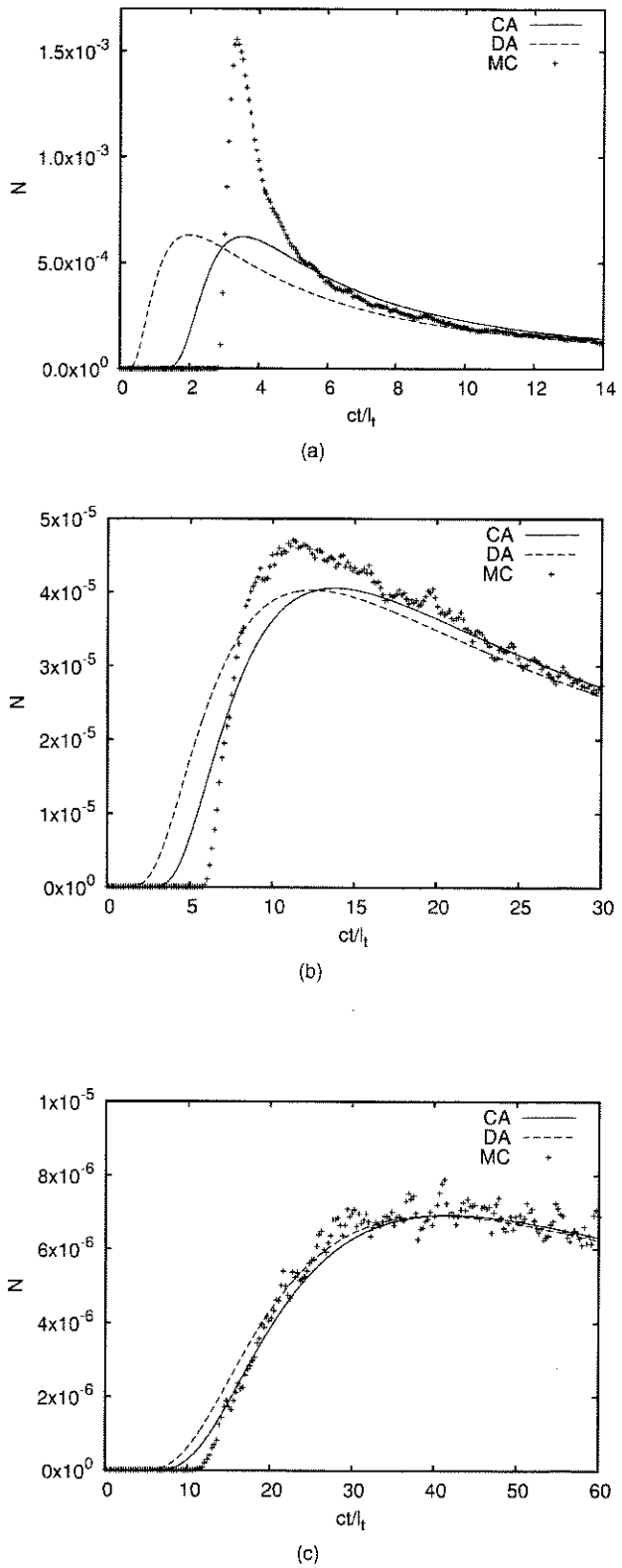

FIG. 3. Photon density at positions (a) $(0,0,3l_t)$, (b) $(0,0,6l_t)$, and (c) $(0,0,10l_t)$ vs time normalized to a unit source in an infinite medium. The source is incident along the positive z axis at the origin of the coordinate system and at time zero. The three curves are computed by the diffusion approximation (DA), the cumulant approximation (CA), and the Monte Carlo method (MC), respectively.

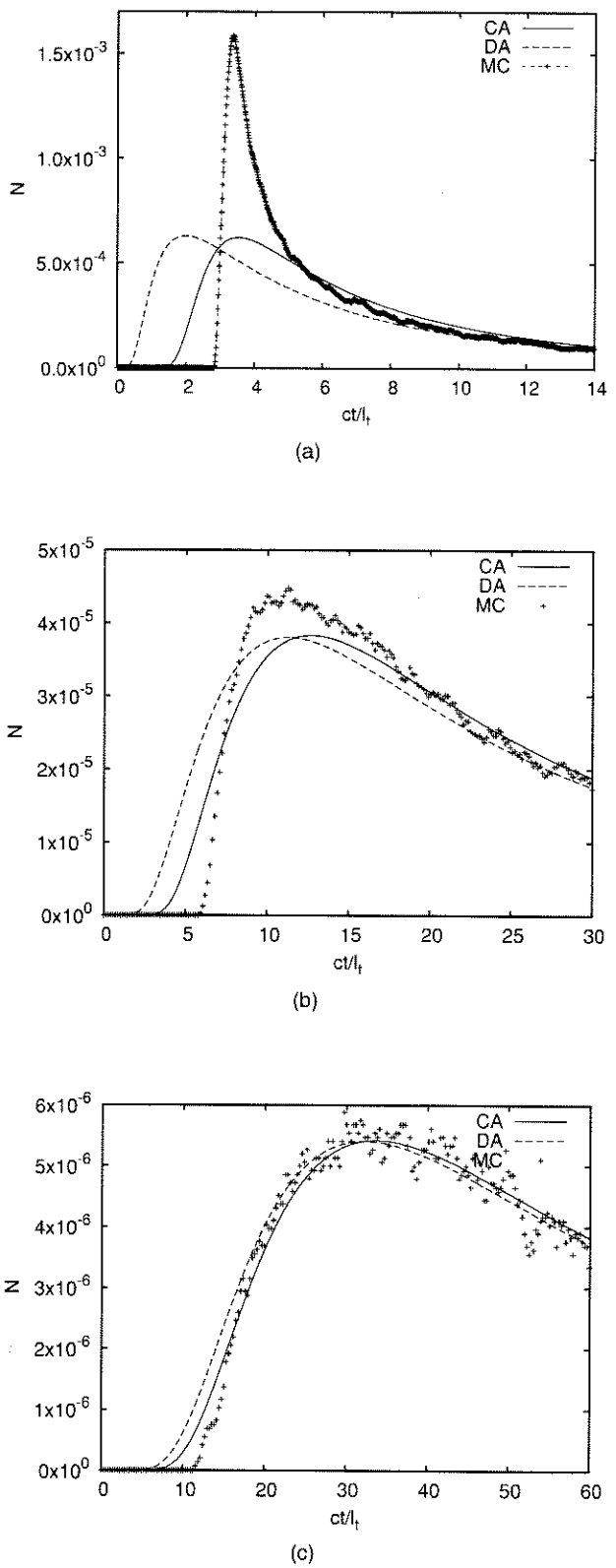

FIG. 4. Photon density at positions (a) $(0,0,3l_t)$, (b) $(0,0,6l_t)$, and (c) $(0,0,10l_t)$ vs time normalized to a unit source in a semi-infinite medium. The source is incident normal to the surface of the medium and along the positive z axis at the origin of the coordinate system and at time zero.

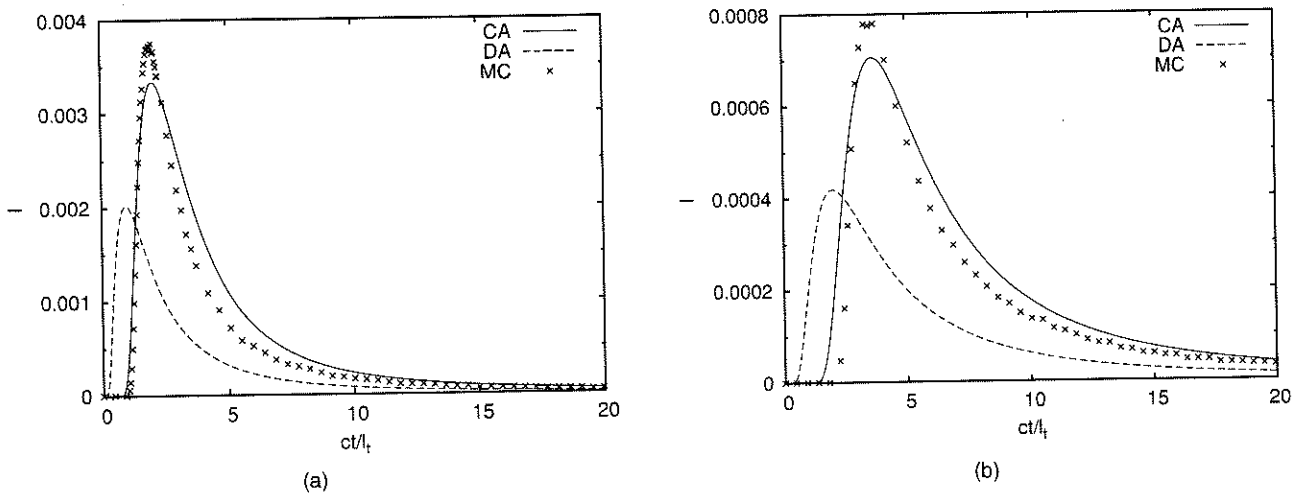

FIG. 5. The backscattered photon intensity $I(\mathbf{r},-\hat{z},t)$ at positions (a) $(0,l_t,0)$ and (b) $(0,2l_t,0)$ on the boundary of a semi-infinite medium vs time normalized to a unit source in a semi-infinite medium. The source is incident normal to the surface of the medium and along the positive z axis at the origin of the coordinate system and at time zero.

three methods begin to agree with each other pretty well and the cumulant approximation is better than the diffusion approximation. The difference between results from DA, CA, and MC is negligible when the distance is $10l_t$ or larger.

The calculations using DA, CA, and MC are performed again for a semi-infinite medium with its boundary at $z=0$, whose optical parameters are taken to be the same as the above infinite medium. The source is incident at the origin of the coordinate system and along the positive z axis (normal to the surface) at time zero. The effective reflectivity is taken to be zero and an extrapolation length $z_e=0.7l_t$ is used in both DA and CA calculations. Figures 4(a)–4(c) shows the corresponding results for this example. Again CA shows a much better agreement to the MC than DA. Compared with Fig. 3 for the infinite case, the tail of the profiles in Figs. 4(a)–4(c) for the semi-infinite medium is lower due to the presence of an extra negative image source coming from the boundary condition.

As a final example, the backscattered photon intensity $I^{(0)}(\mathbf{r},-\hat{z},t)$ at positions $(0,l_t,0)$ and $(0,2l_t,0)$ on the boundary of the above semi-infinite medium is calculated with use of the three different methods (see Fig. 5). In DA, photons diffuse from the adjusted source position $(0,0,l_t)$ with the constant diffusion coefficient $D=l_t/3$. In CA, back-scattered photons arrive later because the center of photons moves forward along the positive z direction and diffuse from the moving center with a gradually increasing diffusion coefficient from 0 to $l_t/3$. CA agrees well with the Monte Carlo simulation.

C. Weight function for image reconstruction

The response (the change of the scattered wave field) to a unit absorption or scattering inhomogeneity is usually called the weight function or the Jacobian in medical tomography literature. This quantity plays a central role in image reconstruction regardless of which method is used to obtain the inhomogeneity distribution in a medium. Let us rewrite Eq. (9) in the following form:

$$4\pi\delta I(\mathbf{r},\mathbf{s},t|z_0,\mathbf{s}_0)=-c\int d\mathbf{r}'\,\delta\mu_a(\mathbf{r}')w_a(\mathbf{r},\mathbf{s},\mathbf{r}_0,\mathbf{s}_0,t;\mathbf{r}') + \frac{c}{3\mu_s'^2}\int d\mathbf{r}'\,\delta\mu_s'(\mathbf{r}') \times w_s(\mathbf{r},\mathbf{s},\mathbf{r}_0,\mathbf{s}_0,t;\mathbf{r}') \tag{14}$$

with the absorption and scattering weight functions defined as

$$w_a(\mathbf{r},\mathbf{s},\mathbf{r}_0,\mathbf{s}_0,t;\mathbf{r}')=\int_0^t dt' N^{(0)}(\mathbf{r}',t-t'|\mathbf{r},-\mathbf{s})N^{(0)}(\mathbf{r}',t'|\mathbf{r}_0,\mathbf{s}_0)-w_s(\mathbf{r},\mathbf{s},\mathbf{r}_0,\mathbf{s}_0,t;\mathbf{r}')/(3\mu_s'^2)$$

$$\frac{w_s(\mathbf{r},\mathbf{s},\mathbf{r}_0,\mathbf{s}_0,t;\mathbf{r}')}{9\mu_s'^2}=\int_0^t dt' D(t-t')D(t')\nabla_{\mathbf{r}'}N^{(0)}(\mathbf{r}',t-t'|\mathbf{r},-\mathbf{s})\cdot\nabla_{\mathbf{r}'}N^{(0)}(\mathbf{r}',t'|\mathbf{r}_0,\mathbf{s}_0)+\int_0^t dt' D(t') \times\exp[-c\mu_s'(t-t')]N^{(0)}(\mathbf{r}',t-t'|\mathbf{r},-\mathbf{s})\mathbf{s}\cdot\nabla_{\mathbf{r}'}N^{(0)}(\mathbf{r}',t'|\mathbf{r}_0,\mathbf{s}_0)-\int_0^t dt' D(t-t') \times\exp(-c\mu_s't')\mathbf{s}_0\cdot\nabla_{\mathbf{r}'}N^{(0)}(\mathbf{r}',t-t'|\mathbf{r},-\mathbf{s})N^{(0)}(\mathbf{r}',t'|\mathbf{r}_0,\mathbf{s}_0), \tag{15}$$

respectively.

As $N^{(0)}(\mathbf{r},t|\mathbf{r}_0,\mathbf{s}_0)\rightarrow\delta(\mathbf{r}-\mathbf{r}_0-ct\mathbf{s}_0)$ when $t\rightarrow 0$, special attentions must be paid when a numerical integration is carried out for Eq. (15). The range of integration is divided into three areas: $(0,\Delta)$, $(\Delta,t-\Delta)$, and $(t-\Delta,t)$ where $t\gg\Delta>0$. The end corrections from the integration over $(0,\Delta)$ and $(t-\Delta,t)$ to the weight functions integrated over $(\Delta,t-\Delta)$ range are approximately given by

$$e_a(\mathbf{r},\mathbf{s},\mathbf{r}_0,\mathbf{s}_0,t;\mathbf{r}')=\frac{1}{c}N(\mathbf{r}',t|\mathbf{r},-\mathbf{s})\,\delta(x'-x_0)\,\delta(y'-y_0)H(\Delta-\xi)H(\xi)+\frac{1}{c}N(\mathbf{r}',t|\mathbf{r}_0,\mathbf{s}_0)\,\delta(x'-x)\,\delta(y'-y)H(\Delta-\eta)H(\eta)$$
$$-e_s(\mathbf{r},\mathbf{s},\mathbf{r}_0,\mathbf{s}_0,t;\mathbf{r}')/(3\mu_s'^2),$$
$$\frac{e_s(\mathbf{r},\mathbf{s},\mathbf{r}_0,\mathbf{s}_0,t;\mathbf{r}')}{9\mu_s'^2}=-\frac{D(t)}{c}\left(1-\frac{\partial D(t)}{c\,\partial t}\bigg|_{t=\xi}\right)\mathbf{s}_0\cdot\nabla_{\mathbf{r}'}N(\mathbf{r}',t|\mathbf{r},-\mathbf{s})\,\delta(x'-x_0)\,\delta(y'-y_0)H(\Delta-\xi)H(\xi)+\frac{D(t)}{c}$$
$$\times\left(1-\frac{\partial D(t)}{c\,\partial t}\bigg|_{t=\eta}\right)\mathbf{s}\cdot\nabla_{\mathbf{r}'}N(\mathbf{r}',t|\mathbf{r}_0,\mathbf{s}_0)\,\delta(x'-x)\,\delta(y'-y)H(\Delta-\eta)H(\eta),\qquad(16)$$

where $\mathbf{r}'=\mathbf{r}_0+c\xi\mathbf{s}_0=\mathbf{r}-\eta c\mathbf{s}$ is the position of the inhomogeneity, $\mathbf{s}$ and $\mathbf{s}_0$ are assumed to be along the positive or negative z axis, and H is the Heaviside function. In the following calculations, the refractive index of the medium is assumed to be 1.33; the absorption and scattering coefficients of the medium are assumed to be 0.003 mm^{-1} and 10 mm^{-1}, respectively, and the scattering anisotropy 0.9, providing a transport mean free path $l_t=1$ mm. The offset Δ is taken to be 0.1 ps when more than 99% of the photon packet still concentrates within a cubic volume $(0.01l_t)^3$. The weight function from a cubic of volume $(0.01l_t)^3$ is calculated using the DCUHRE algorithm [27].

The weight functions for a semi-infinite medium are shown in Fig. 6 for absorption and scattering inhomogeneities. The backscattered photons (propagating along negative z axis) are detected by a detector placed at a position $(0,2l_t,0)$, off two transport mean free path from the source. Figures 6(a) and 6(c) show the response to an inhomogeneity at $(0,0,z)$ positions which is in the propagation direction of the source at delay 50 ps and 500 ps. The CA shows a much stronger response from the inhomogeneity in the propagation direction of and close to the source than the diffusion approximation. Both absorption and scattering weight functions from CA reveal a peak at about $0.03l_t$. This peak originates from the initial ballistic motion of the incident photon. In a short time after the photon is launched $(t\rightarrow 0)$, the photon packet will be positioned at $z^*=ct$ with a spread of half-width $\approx\sqrt{4D(t)ct}=2ct\sqrt{ct/(3l_t)}$, hence the presence of an absorption or scattering inhomogeneity at position $(0,0,z<z^*)$, sitting in the ballistic path of the photon, will significantly reduce the number of backscattered photons received by the detector [$w_a>0$ and $w_s<0$ in Eq. (14)]. In Figs. 6(b) and 6(d) where the inhomogeneity is placed at $(0,l_t,z)$ mm positions, not sitting in the ballistic path of the photon, this peak is gone.

The diffusion approximation is invalid when the inhomogeneity is too close to the source or the detector. Nevertheless, the weight function from DA is plotted over the full z range for comparison. A peak is found in the absorption weight function [Fig. 6(a)] and a crossing of zero in the scattering weight function [Fig. 6(c)] at $z=l_t$, because of the artificial adjustment of the source position to one transport mean free path into the medium and the singularity of the Green's function in DA when the inhomogeneity and the source overlap.

A larger disagreement between CA and DA is observed in the scattering weight function than in the absorption weight function. The absorption weight functions from CA and DA agree with each other relatively well except for a region of depth of l_t near the surface when the inhomogeneity is in the propagation direction of the source, or in the field of view of the detector. The scattering weight functions from CA and DA disagree significantly within the region of depth of at least $2l_t$ close to the surface. The deepest position that can be detected by the detector at time t is roughly $ct/2$. This condition is better observed by CA because CA shows a faster decay rate of both the absorption and scattering weight functions with the increase of the depth [Figs. 6(a)–6(d)].

The absorption and scattering weight functions for a slab is shown in Fig. 7. The slab has the same optical parameter as the semi-infinite medium. The thickness of the slab is $d=30l_t$. The source is at the origin $(0,0,0)$. The detector is placed on the opposite side of the slab, $(0,0,30l_t)$, in the propagation direction of the source. The weight functions by the cumulant approximation and the diffusion approximation are strictly symmetric about the plane $z=d/2$. The agreement between CA and DA for the absorption weight function is better than for the scattering weight function. Both CA and DA produce close results for the inhomogeneity not located near the boundary. When the inhomogeneity is placed along the line $(0,0,z)$, in the propagation direction of the source and in the field of view of the detector, two peaks at about $0.03l_t$ and $d-0.03l_t$ appear in CA; two peaks in the absorption weight function [Fig. 7(a)] and two crossings of zero in the scattering weight function [Fig. 7(c)] appear in DA at l_t and $d-l_t$.

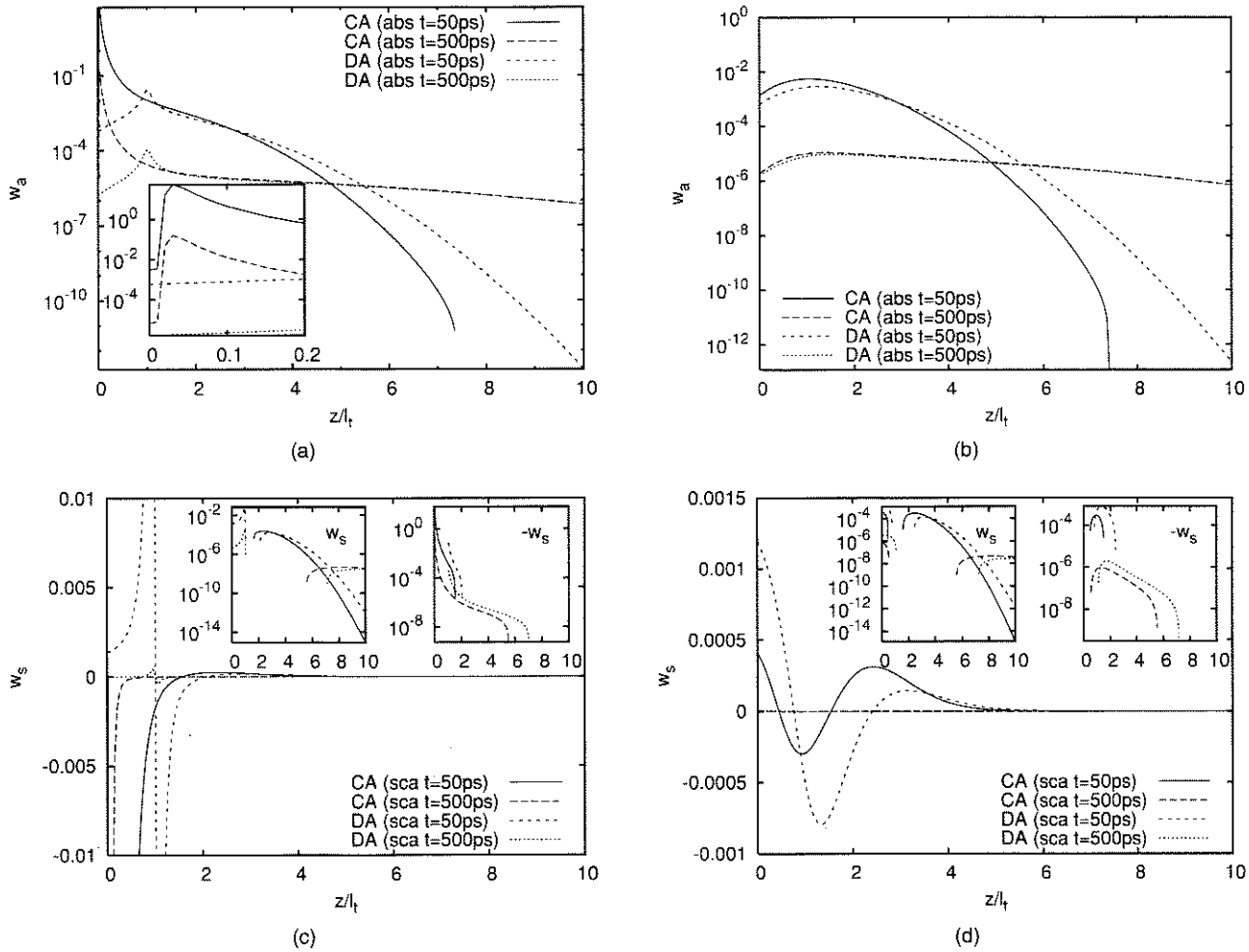

FIG. 6. Weight functions for a semi-infinite medium where the inhomogeneity is (a) absorption and (c) scattering at $(0,0,z)$, in the propagation direction of the source; (b) absorption and (d) scattering at $(0,l_t,z)$, off by one transport mean free path. Profiles at two delay times $t=50$ ps and $t=500$ ps are plotted for both the cumulant approximation (CA) and the diffusion approximation (DA). The insets replot the weight functions in a logarithm scale.

III. DISCUSSION

We attribute the formation of a peak very close to the surface but not on the surface (about $0.03l_t$ into the medium) of the absorption and scattering weight function in the cumulant approximation to the initial ballistic motion of the incident photon. The photon penetrates into the medium with an initial speed of c and with its center approaching and stopping at one transport mean free path into the medium. Hence the effect is only significant when the inhomogeneity is in the propagation direction of the source or in the field of view of the detector, and the peak response shifts away from the surface of the medium.

The diffusion approximation requires one to adjust the position of the source to compensate for the initial ballistic motion of the photon [8,28,29]. From our more accurate result Eq. (9), the source and the detector terms appear in a form of $N^{(0)}(\mathbf{r}',\tau|\mathbf{r},-\mathbf{s})$ and $N^{(0)}(\mathbf{r}',\tau|\mathbf{r}_0,\mathbf{s}_0)$, respectively. The source and the detector approach gradually and stop at $\mathbf{r}_0+l_t\mathbf{s}_0$ and $\mathbf{r}-l_t\mathbf{s}$, respectively, with the increase of time where $\mathbf{s}_0$ and $\mathbf{s}$ are the propagating directions of the incident and outgoing photon. The positioning of both the source and the detector for one transport mean free path into the medium is hence mandatory if the diffusion approximation is used. The curves for DA in Figs. 6 and 7 are calculated using this adjustment. The DA will deviate from the CA significantly over the full range of depth if the adjustment on the position of the source or the detector is not performed.

The diffusion approximation for image reconstruction substantially underestimates the contribution to the emission measurement from the inhomogeneity in the propagation direction of and close to the source, or in the field of view and close to the detector. This error may distort the signal from the inhomogeneity inside the medium because the weight function near surface is usually much larger than that inside, and may lead to a failure in image reconstruction. The high response from the region near surface is not desirable when the inhomogeneity inside the medium is to be detected in the transmission or backscattering measurements. The cancella-

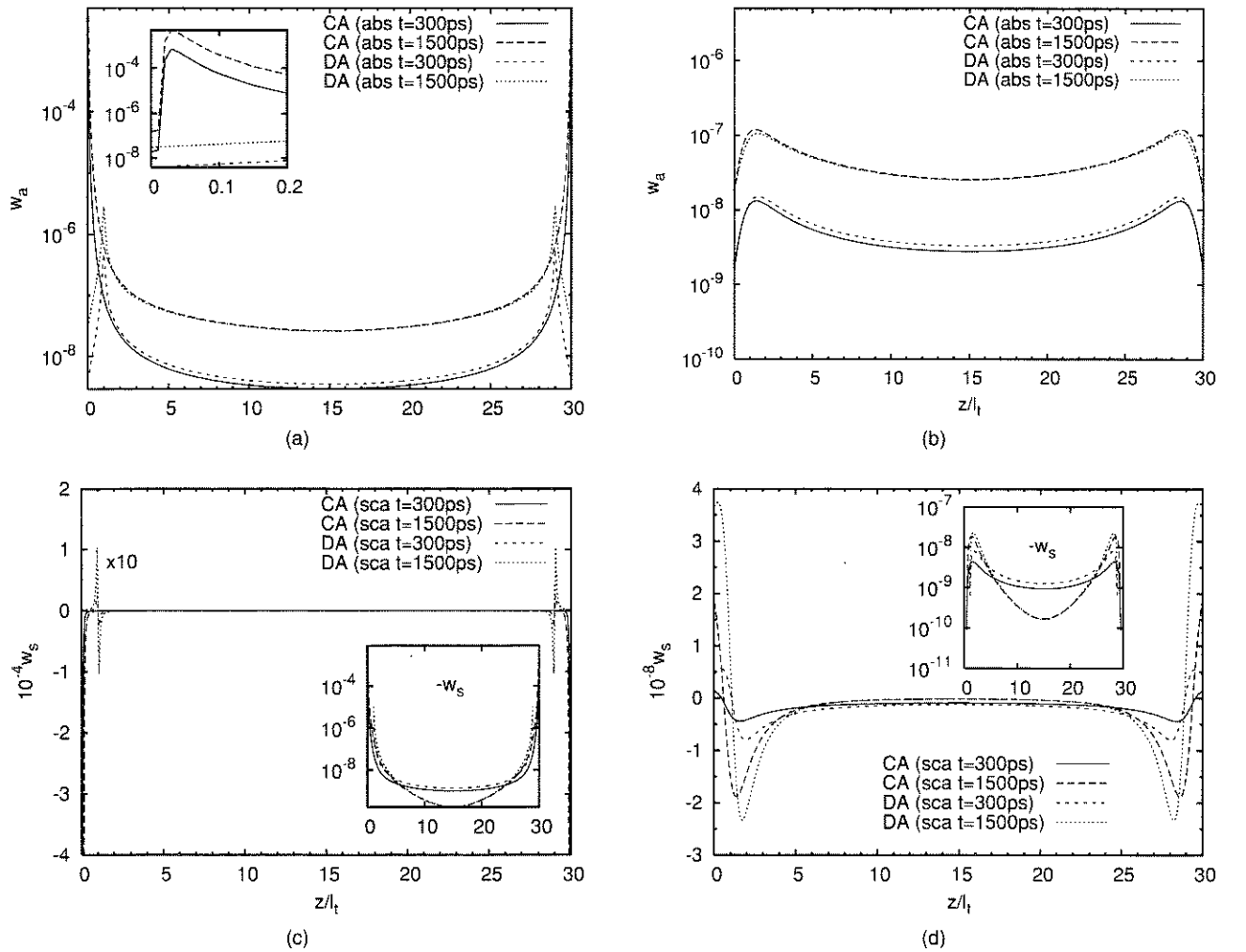

FIG. 7. Weight function for a slab where the inhomogeneity is (a) absorption and (c) scattering at $(0,0,z)$, in the propagation direction of the source, (b) absorption and (d) scattering at $(0,l_t,z)$, off by one transport mean free path. Weight functions calculated from the cumulant (CA) and diffusion (DA) approximations are plotted for time delays of $t=300$ ps and $t=1500$ ps. The insets replot the weight functions in a logarithm scale.

tion between multiple measurements using nearby wavelengths may help reduce this effect.

Other attempts to obtain a better approximation to radiative transfer in turbid media were made by various authors such as Ishimaru's diffusion approximation [30,31], the telegrapher equation of Durian *et al.* based on the two stream theory [32], Gershenson's time-dependent equation in the diffusion limit using a higher-order angular expansion [6], and non-Euclidean diffusion equation of Polishchuk *et al.* [33]. The advantage of this cumulant approximation is that it provides a clear picture of photon migration for an incident collimated beam from early to later times and that it gives the *exact* center and the *exact* spread of the photon cloud at both early and later times by only using a second-order cumulant approximation.

In conclusion, we have presented a cumulant approximation to radiative transfer, which provides an analytical tool to describe photon migration at both early and later times—from the initial ballistic motion till the final diffuse regime. To a second-order cumulant, the solution agrees with the Monte Carlo simulation at later times and provides a correct peak position in time for photon arrivals at early times, in both an infinite medium and a bounded medium with a planar geometry. The initial ballistic motion of photon produces a strong peak in the response from absorption and/or scattering inhomogeneities, which are in the propagation direction of and close to the source, or in the field of view of and close to the detector, at both early and later times.

ACKNOWLEDGMENTS

This work was supported in part by the U.S. Army Medical Research Material Command, NASA Institutional Research Award, the New York State Office of Science, Technology and Research, and the U.S. Department of Energy.

[1] S. Chandrasekhar, *Radiation Transfer* (Oxford University Press, Oxford, 1950).
[2] J. J. Duderstadt and W. R. Martin, *Transport Theory* (Wiley, New York, 1979).
[3] A. Ishimaru, *Wave Propagation and Scattering in Random Media* (Academic, New York, 1978), Vols. I and II.
[4] C. Cercignani, *The Boltzmann Equation and its Applications*, Applied Mathematical Sciences Vol. 67 (Springer-Verlag, Berlin, 1988).
[5] G. D. Mahan, J. Math. Phys. **36**, 6758 (1995).
[6] M. Gershenson, Phys. Rev. E **59**, 7178 (1999).
[7] K. M. Yoo, F. Lin, and R. R. Alfano, Phys. Rev. Lett. **64**, 2647 (1990).
[8] M. S. Patterson, B. Chance, and B. C. Wilson, Appl. Opt. **28**, 2331 (1989).
[9] S. Fantini *et al.*, Proc. SPIE **2389**, 204 (1995).
[10] J. Opt. Soc. Am. A **14**, 136 (1997), special issue on diffusing photons in turbid media, edited by A. G. Yodh, B. Tromberg, E. Sevick-Muraca, and D. Pine.
[11] J. C. Hebden, S. R. Arridge, and D. T. Delpy, Phys. Med. Biol. **42**, 825 (1997).
[12] S. R. Arridge and J. C. Hebden, Phys. Med. Biol. **42**, 841 (1997).
[13] *Proceedings of Inter-Institute Workshop on In Vivo Optical Imaging at the NIH*, edited by A. H. Gandjbakhche (Optical Society of America, Washington, D.C. 1999).
[14] W. Cai, M. Lax, and R. R. Alfano, Phys. Rev. E **61**, 3871 (2000).
[15] W. Cai, M. Lax, and R. R. Alfano, J. Phys. Chem. B **104**, 3996 (2000).
[16] S. H. Ma, *Statistical Mechanics* (World Scientific, Philadelphia, 1985).
[17] M. Wu, W. Cai, M. Lax, and R. R. Alfano, Opt. Lett. **26**, 1066 (2001).
[18] S. R. Arridge, Appl. Opt. **34**, 7395 (1995).
[19] J. X. Zhu, D. J. Pine, and D. A. Weitz, Phys. Rev. A **44**, 3948 (1991).
[20] G. Popescu, C. Mujat, and A. Dogariu, Phys. Rev. E **61**, 4523 (2000).
[21] R. C. Haskell, I. O. Svaasand, T.-T. Tsay, T.-C. Feng, M. S. McAdams, and B. J. Tromber, J. Opt. Soc. Am. A **11**, 2727 (1994).
[22] J. C. J. Paasschens and G. W. 't Hooft, J. Opt. Soc. Am. A **15**, 1797 (1998).
[23] S. A. Prahl, M. Keijzer, S. L. Jacques, and A. J. Welch, Proc. SPIE **IS-5**, 102 (1989).
[24] L. H. Wang, S. L. Jacques, and L. Q. Zheng, Comput. Methods Programs Biomed. **47**, 131 (1995).
[25] L. G. Henyey and J. L. Greenstein, Astrophys. J. **93**, 70 (1941).
[26] R. Y. Rubinstein, *Simulation and the Monte Carlo Method* (Wiley, New York, 1981).
[27] J. Berntsen, T. O. Espelid, and A. Genz, ACM Trans. Math. Softw. **17**, 452 (1991).
[28] J. S. Maier and E. Gratton, Proc. SPIE **1888**, 440 (1993).
[29] Y. Tsuchiya, K. Ohta, and T. Urakami, Jpn. J. Appl. Phys., Part 1 **34**, 2495 (1995).
[30] A. Ishimaru, J. Opt. Soc. Am. **68**, 1045 (1978).
[31] A. Ishimaru, J. Opt. Soc. Am. A **1**, 506 (1984).
[32] D. J. Durian and J. Rudnick, J. Opt. Soc. Am. A **14**, 940 (1997).
[33] A. Y. Polishchuk and R. R. Alfano, Opt. Lett. **21**, 916 (1996).